BROWNIAN DYNAMICS OF TETHERED POLYMERS IN FLOW

R. RZEHAK,[1] D. KIENLE,[1] T. KAWAKATSU[2] AND W. ZIMMERMANN[1,3]

[1] *IFF and FORUM Modellierung, Forschungszentrum Jülich, D-52425 Jülich*
[2] *Dept. Comput. Sci. Eng. Nagoya University, Nagoya 464-8603, Japan*
[3] *Theoretische Physik, Universität des Saarlandes, D-66041 Saarbrücken*
E-mail: wz@lusi.uni-sb.de

The shape and the dynamics of tethered polymers in flow are described by bead–spring models taking into account the hydrodynamic interaction and the excluded volume effects. The Brownian dynamics of these bead–spring models is simulated by replacing the discretized Langevin equation with a scheme which introduces artificial inertia for the beads. With this scheme the preservation of the Boltzmann distribution is guarateed in leading order and the integration timestep can be chosen up to a factor of 10 larger. Besides various applications of this scheme, we devise an efficient way to calculate the relaxation spectrum and -modes from the simulation data using the Karhunen–Loève method.

1 Introduction

Polymers exhibit a hierarchy of time and length scales which covers a very wide range. There are modes of the polymer dynamics with relaxation times which are as slow as the macroscopic hydrodynamic modes. In this case the microscopic and macroscopic degrees of freedom do not decouple in a simple manner as for simple fluids like water. The viscoelasticity of polymer solutions is a consequence of this coupling of very different length and time scales [1,2,3].

The behavior of polymers in flowing solution has already been investigated experimentally for a long time but only by volume averaging measurements such as light scattering, birefringence, rheometry and small angle neutron scattering. An understanding of viscoelasticity, however, requires an analysis of the nonlinear interaction between individual polymers and the flow field. Two elementary processes seem to be crucial for the interaction: How does a flow field deform a polymer and how does the deformed polymer perturb the flow field?

Only recently a huge step forward in understanding the flow-induced polymer deformation has been achieved by studying single DNA molecules. DNA is much larger than synthetic polymers and can be manipulated with optical tweezers. When decorated by fluorescent dyes, the action of flows on the polymer can be followed under an optical microscope[4−7].

Theoretically the deformation of a tethered polymer in flow can be described by various models. These are for instance the dumbbell model[2] and various kinds of blob models[8−13] which neglect a large number of internal degrees of freedom of the polymer. More details are kept in bead–spring models where the actual polymer is replaced by a string of beads connected by springs, cf. fig. 1, each of which corresponds to at least one Kuhn segment for a flexible chain[3]. Such bead–spring models have been investigated so far only with various averaging approximations for the hydrodynamic interactions (**HI**) between the beads [14,15,16]. Here and in Refs. [10, 11] the HI are described in the so-called Oseen-approximation without any averaging. At first sight these simulations with HI require $\mathcal{O}(N^3)$ operations,

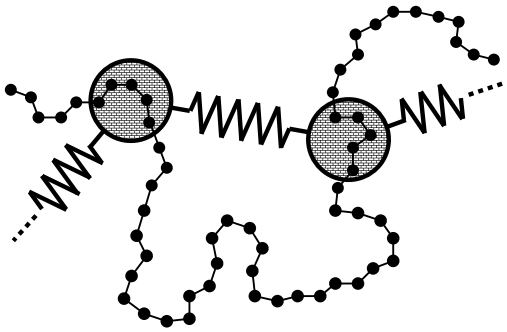

Figure 1. Sketch of the coarse–graining procedure leading to the bead–spring model. The small solid circles represent chemical groups in the backbone of the polymer with the solid lines indicating chemical bonds between them. The large shaded circles are the beads which are connected by springs reflecting the entropic elasticity of the subchain.

but with a suitable approximation the operation count is reduced to $\sim \mathcal{O}(N^{2.25})$ operations, as described in appendix B.

Simulations of the model equations as described in sec. 2 provide the shape of the flow-deformed polymer as well as the perturbation of the flow field and they show that polymers in flow are neither impenetrable as assumed in former blob models[8] nor free draining.

Another central issue in polymer dynamics is the determination of the spectrum of relaxation times and modes of a polymer[1,3]. The former provides the link between the microscopic dynamics of the polymers and macroscopic viscoelastic continuum theory[17]. Analytically the relaxation spectrum can be calculated only for the simplest polymer models, namely those of Rouse and Zimm [18,19,20]. Both of these models share the feature that they yield linear equations governing the motion of the polymer. For more realistic nonlinear polymer models one encounters a fundamental difficulty [1,21,22]: The nonlinearity leads to a coupling of modes and independently relaxing modes like in the linear case do not exist.

A common way out of this situation is to simply assume that the amplitudes of the Rouse modes contain useful information on the relaxation of the polymer chain even in the nonlinear case. The relaxation times are then determined from an exponential fit to the timeseries of these amplitudes. Even if one accepts the premise of using the Rouse modes, the determination of the relaxation times is tedious and error-prone so that in practice only the few longest relaxation times can be obtained this way. Another approach which aims at the relaxation spectrum directly [4] is to apply an inverse Laplace transform to a single timeseries of some observable like the end–to–end distance. This, however, is an ill-conditioned problem due to the presence of noise in the data and requires the use of special regularization techniques [23,24]. The results then in general depend strongly on the regularization parameter. Therefore the efficient and reliable computation of relaxation spectra is also a very practical problem.

Here we suggest a way to determine the relaxation spectrum and -modes of

polymers which solves both of the problems discussed above using the Karhunen–Loève (KL–) method [25].

2 Bead–Spring Models for Polymer Dynamics

In order to study the long-time dynamics of polymers in dilute solution, coarse–grained models are used because atomistic models of long polymer chains are intractable even numerically with present day computing equipment. A common class of such models are the so-called bead–spring models[26] where coares–graining is achieved by replacing a subchain of a real polymer by a bead and a spring with a suitable force–elongation law [3,27]. Friction and mass of the subchains are lumped into the beads as depicted in fig. 1. The solvent acts as a heat bath which causes a stochastic motion of the polymer.

Usually one considers the motion on the diffusive timescale only, *i.e.* bead inertia are neglected[28]. The equation of motion for the position of the i–th bead ($i = 1 \ldots N$) is then obtained from a balance between all forces acting on the beads. These forces comprise viscous drag forces $\mathbf{F}^{\mathrm{H}}$ on one side and spring– and stochastic forces $\mathbf{F}^{\Phi}$, $\mathbf{F}^{\mathrm{S}}$ on the other:

$$-\mathbf{F}_i^{\mathrm{H}} = \mathbf{F}_i^{\Phi} + \mathbf{F}_i^{\mathrm{S}} \,. \tag{1}$$

The drag forces are proportional to the difference between the velocity of the bead, $\mathbf{V}_i$, and the flow velocity at its position, $\mathbf{u}_0(\mathbf{R}_i)$:

$$-\mathbf{F}_i^{\mathrm{H}} = \zeta \; (\mathbf{V}_i - \mathbf{u}_0(\mathbf{R}_i)) \,. \tag{2}$$

The single bead friction coefficient ζ is given by Stokes law, *i.e.* $\zeta = 6\pi\eta a$ where η is the solvent viscosity and a is the effective hydrodynamic radius of a bead. In thermal equilibrium of course $\mathbf{u}_0 \equiv \mathbf{0}$. The stochastic forces are related to the dissipative drag by the fluctuation dissipation theorem in order to ensure the correct equilibrium distribution. We have

$$\mathbf{F}_i^{\mathrm{S}} = \sqrt{2k_{\mathrm{B}}T\,\zeta}\;\xi_i \tag{3}$$

where T is the solvent temperature, k_{B} is the Boltzmann constant and ξ_i is an uncorrelated gaussian white noise with zero mean:

$$\left\langle \xi(t)\; \xi^T(t') \right\rangle = \delta(t-t')\,\mathbf{1} \,. \tag{4}$$

Taking velocities and positions of *all* beads together as single supervectors for the velocity $\mathbf{V}$ and position $\mathbf{R}$, the equations of motion may be written in the following general form:

$$\mathbf{V} \equiv \frac{\partial}{\partial t}\mathbf{R} = \mathbf{u}_0(\mathbf{R}) + \mathbf{H}\cdot(-\nabla_{\mathbf{R}}\,\Phi) + \sqrt{2k_{\mathrm{B}}T\,\mathbf{H}}\;\xi \,. \tag{5}$$

Here we introduced a potential Φ for the spring forces and the mobility $\mathbf{H}$, which is the inverse of the friction coefficient, ζ^{-1}. In the most general case to be discussed later on, $\mathbf{H}$ will no longer be a simple scalar but a tensor which couples all beads. Boundary conditions are implemented by introducing additional beads with indices $i = 0, N+1$ which do not participate in the dynamics. Then for free chain ends we have $\mathbf{R}_0 = \mathbf{R}_1$ and $\mathbf{R}_{N+1} = \mathbf{R}_N$ while for fixed ends $\mathbf{R}_0$ and $\mathbf{R}_{N+1}$ are constant.

The Rouse model[18] is the simplest conceivable polymer model which embodies only the chain connectivity by assuming harmonic springs, *i.e.* by using in eq. (5),

$$\Phi \equiv \Phi_{\rm H} = \sum_i \frac{1}{2}\, k_{\rm H}\, |\mathbf{R}_{i+1} - \mathbf{R}_i|^2 \,. \tag{6}$$

The mobility in the Rouse model is simply a scalar, namely the inverse of the single bead friction coefficient, *i.e.* $\mathbf{H} = \zeta^{-1}\, \mathbf{1}$. All of the above assumptions are tacitly introduced in order to make the equation of motion eq. (5) linear so that it may be solved analytically.

There are three obvious refinements all of which render the equation of motion eq. (5) nonlinear. These are a finite extensibility of the springs (FE), the excluded volume of the beads (EV), which may be chosen such that the chain cannot cross itself, and hydrodynamic interactions between the beads (HI).

Since chemical bonds have a fixed length, real polymers are inextensible. This can be modeled by a nonlinear spring law which keeps the stretching of the springs small even for large forces. Rather common in simulations is the phenomenological FENE (**F**initely **E**xtensible **N**onlinear **E**lastic) spring law[29] with the potential

$$\Phi \equiv \Phi_{\rm F} = -\sum_i \frac{1}{2}\, k_{\rm F}\, R_{\rm F}^2 \ln\!\left(1 - \frac{|\mathbf{R}_{i+1} - \mathbf{R}_i|^2}{R_{\rm F}^2}\right). \tag{7}$$

Here $k_{\rm F}$ is the force constant and $R_{\rm F}$ is the maximum extension of the spring. Another approach is to make the chain completely unstretchable by replacing the springs with rigid rods. In numerical simulations this may be achieved to a good approximation by augmenting the FENE spring law by a nearest–neighbor repulsion of the form described in eq. (8) below [30]. Obviously the effects of finite extensibility are most important when the polymer is driven far from equilibrium where the chain may be strongly stretched.

The excluded volume (EV) effect arises because different beads cannot occupy the same region in space. This is modeled by a repulsive interaction between any pair of beads as described *e.g.* by a truncated Lennard–Jones potential[30]

$$\Phi_{\rm LJ} = \begin{cases} \displaystyle\sum_{i,j} 4\epsilon \left(\left(\frac{\sigma}{|\mathbf{R}_j - \mathbf{R}_i|} \right)^{12} - \left(\frac{\sigma}{|\mathbf{R}_j - \mathbf{R}_i|} \right)^{6} + \frac{1}{4} \right) & \text{for } |\mathbf{R}_j - \mathbf{R}_i| < R_{\rm LJ} \\ 0 & \text{for } |\mathbf{R}_j - \mathbf{R}_i| \geq R_{\rm LJ} \end{cases} \tag{8}$$

Here ϵ and σ define energy and length scales of the excluded volume interaction and $R_{\rm LJ} = 2^{1/6}\sigma$ is the minimum of the conventional 6-12 Lennard–Jones potential. This term is included in the potential Φ in eq. (5) along with the spring potential. For a suitable choice of the parameters the bead–spring chain becomes self–avoiding like real polymers. The effects of excluded volume are most prominent in or close to thermal equilibrium where the polymer chain assumes a coil shape. Far from equilibrium, where the polymer chain is strongly stretched and the beads are far apart from each other, the excluded volume force tends to zero.

The hydrodynamic interaction (HI) is an effective interaction between any pair of beads which is mediated by the solvent. It arises in the following way: If the

solvent exerts a drag force on a bead then by virtue of Newton's third law there must be a drag reaction force of the same strength but with reverse direction acting as a driving force for the solvent. According to eq. (1) the average of this force is given by the potential force $-\nabla_{\mathbf{R}}\,\Phi$. Neglecting the finite bead diameter – *i.e.* idealizing the drag reaction force as a point force – and using the linear equations of Stokes flow for the solvent dynamics, one can derive a general expression for the perturbation $\mathbf{u}'$ of the imposed flow field resulting from the drag reaction forces of all beads[31,3,27],

$$\mathbf{u}'(\mathbf{R}_i) = \sum_{j\neq i} \Omega(\mathbf{R}_i - \mathbf{R}_j)\cdot(-\nabla_{\mathbf{R}_j}\,\Phi)\,. \tag{9}$$

The i–th bead is excluded from the sum on the *rhs* of eq. (9) in order to suppress unphysical hydrodynamic self–interactions. The Stokes friction force on bead i as given by eq. (2) now arises from the bead velocity relative to the *perturbed* flow field $\mathbf{u}_0 + \mathbf{u}'$. Using this perturbed flow field instead of $\mathbf{u}_0$ alone in eq. (5) and collecting all terms containing $-\nabla_{\mathbf{R}}\,\Phi$, one identifies the components of the mobility, which has now become a conformation dependent supermatrix, as

$$\mathbf{H}_{ij} = \begin{cases} \frac{1}{\zeta}\,\mathbf{1} & \text{for} \quad i = j \\ \\ \Omega(\mathbf{R}_i - \mathbf{R}_j) & \text{for} \quad i \neq j \end{cases}\,. \tag{10}$$

Here the Oseen tensor[3] is nothing but the Greens function for Stokes flow,

$$\Omega(\mathbf{r}) = \frac{1}{8\pi\eta|\mathbf{r}|}\,(\mathbf{1} + \hat{\mathbf{r}}\hat{\mathbf{r}}^T)\,. \tag{11}$$

It suffers from the deficiency that it becomes non-positive at small bead separations. Therefore it is necessary to introduce EV along with HI[10] or to use a regularization of the Oseen tensor[32]. So far we considered deterministic forces only. In order to complete the equation of motion for the case with HI, we need to specify the stochastic forces. Fortunately it turns out that the fluctuation dissipation theorem for this case has precisely the same form as before[33].

The collective effect of the hydrodynamic interactions is often condensed in the so-called non–draining assumption, *i.e.* the assumption that the polymer coil may be replaced by a sphere with some effective radius into which the external flow does not penetrate. This assumption is inspired by Zimm's calculation of the diffusion coefficient of a polymer coil with HI[19] which is given by an expression similar to that of a hard sphere[3]. Apart from additional approximations in the calculation (see below) this evidence seems rather scarce support for the conclusion drawn. Only recently the perturbed flow field has been calculated directly [11] and this calculation revealed that the flow is weakened inside the polymer coil but not completely suppressed as shown in fig. 2. Furthermore there is a significant penetration depth where the flow remains strong and a large long range effect that are neglected in the simple traditional picture.

If any of the three effects discussed above is to be included in the model without further approximations one has to rely on numerical simulation in order to solve the equation of motion. Only if we restrict ourselves to the Rouse model with HI, an

approximate treatment becomes possible by replacing $\mathbf{H}(\mathbf{R})$ with its equilibrium average. This so-called preaveraging approximation has the effect of linearizing the equation of motion again. This procedure was proposed by Zimm[19], wherefore it is referred to as the Zimm model, who also obtained an expression for the relaxation spectrum. The relaxation modes, however, cannot be found in closed form [20,22]. Far from equilibrium the simple preaveraging approximation obviously breaks down. Various other approximation schemes have been proposed which avoid the use of the equilibrium distribution but which still lead to linear equations [14,15,16].

Since a direct time discretization in eq.(5) may lead to a violation of the equilibrium distribution, we introduce an artificial mass m for all beads as discussed in appendix A. This equation with inertia is integrated with a velocity–Verlet algorithm as follows:

$$\begin{aligned}
\mathbf{R}(t_n + h) &= \mathbf{R}(t_n) + \mathbf{V}(t_n)\, h + \frac{h^2}{2m}\, \mathbf{F}(t_n) \\
m\mathbf{V}(t_n + h) &= m\mathbf{V}(t_n) + \frac{h}{2m}\, (\mathbf{F}(t_n + h) + \mathbf{F}(t_n)) \qquad (12) \\
\mathbf{F}(t_n) &= \zeta \left(\sqrt{2k_{\mathrm{B}}T\, \mathbf{H}(\mathbf{R}(t_n))}\ \Xi(t_n)\, \frac{1}{\sqrt{h}} \right. \\
&\qquad \left. - \left(\mathbf{H}(\mathbf{R}(t_n))\, \frac{\partial \Phi}{\partial \mathbf{R}(t_n)} + \mathbf{V}(t_n) \right) \right) \qquad (13)
\end{aligned}$$

Here $h = t_{n+1} - t_n$ is the time step of integration. Formally this scheme is quite similar to that used in MD–simulations with a Langevin–thermostat, whereas its interpretation is different[34,30]. Noise and dissipation in the MD-simulations are a purely artificial device which is used to simulate a canonical ensemble while the masses of the particles represent true physical quantities. In our case in contrast the masses of the particles are introduced as a computational device to speed up the simulation while the stochastic and dissipative forces represent the solvent degrees of freedom, which do not appear explicitly in the equations of motion.

In the simulation we keep the temperature at $k_BT = 1.0$. Together with the values for the friction coefficient, $\zeta = 1.0$, and the bond length, $b = 1.0$ for harmonic springs and $b = 0.961$ for FENE springs, this fixes the units of energy, force, length etc. . The choice $\eta = 0.2$ for the solvent viscosity, with the bead radius a determined from $\zeta = 6\pi\eta a$, results in a value of $h^* = \sqrt{\frac{3}{\pi}}\frac{a}{b} \approx 0.25$ for the dimensionless parameter h^* measuring the strength of the HI. This value is compatible with other work[22].

Several tests of the numerical scheme with respect to the equilibrium distribution of the bond length for the linear and nonlinear springs and the scaling of the root–mean–square end–to–end distance as a function of the number of beads are described in appendix C. The agreement with analytical solutions for these equilibrium properties is nearly perfect. A comparison between results of the direct discretization and integration of eq. (5) and the scheme eq. (12) shows that the latter allows the integration time step h to be chosen by a factor of 10 larger for a certain accuracy of the equilibrium distribution.

3 The Karhunen–Loève Method

The Karhunen–Loève method used here for the determination of the relaxation spectrum and -modes of polymers can be traced back to the 19th century[35]. Since then it has been rediscovered many times in various fields where it goes under different headings[36], *e.g.* principal component analysis in statistics[35] or proper orthogonal decomposition in turbulence[37]. In nonlinear dynamics the name Karhunen–Loève method, which originally referred to the application to stochastic processes[25], is most widely spread.

The essence of the KL–method is as follows (more details are given elsewhere[38]): The eqs. (12) are integrated over a long time and data vectors $\mathbf{x}(\mu) = \mathbf{R}(\mu \cdot \Delta t)$ comprising all bead positions are stored at equidistant time intervals $\mu \cdot \Delta t$.

Then from this time series the mean positions of the beads are calculated

$$\langle \mathbf{R}_i \rangle = \frac{1}{M} \sum_{\mu=1}^{M} \mathbf{R}_i(\mu \cdot \Delta t) \tag{14}$$

as well as the covariance matrix $\mathbf{K}$ which is composed of the 3×3 submatrices

$$\mathbf{K}_{ij} = \langle \left(\mathbf{R}_i - \langle \mathbf{R}_i \rangle\right) \left(\mathbf{R}_j - \langle \mathbf{R}_j \rangle\right)^T \rangle \,. \tag{15}$$

By calculating the eigenvectors ϕ_p and -values λ_p of $\mathbf{K}$, the KL–method yields a basis for the data space.

The usefulness of the KL-method relies on the following properties[39] of the KL–modes ϕ_p and -weights λ_p.

1. The KL–modes form an orthonormal basis of the data space since $\mathbf{K}$ is symmetric, *i.e.* any data vector may be expressed as

$$\mathbf{x}(\mu) = \mathbf{R}(\mu \cdot \Delta t) = \sum_{p=1}^{N} a_p(\mu) \phi_p \,, \tag{16}$$

   where the expansion coefficients a_p are now random variables like x_i.

2. If the data are expressed with respect to the KL–basis their coefficients are uncorrelated, *i.e.*

$$\langle a_p a_q \rangle = \lambda_p \delta_{pq} \,. \tag{17}$$

   This also shows that the KL–weights give the amount of variance contained in the corresponding mode.

3. If the KL–modes are ordered according to decreasing weights then the average error that occurs upon truncation of the expansion eq. (16) at some $k < N$ is smaller than for any other choice of retained modes, i.e.

$$\langle \| \mathbf{x} - \sum_{i=1}^{k} a_p \phi_p \|^2 \rangle < \langle \| \mathbf{x} - \sum_{i=1}^{k} b_p \psi_p \|^2 \rangle \,, \tag{18}$$

   where $\{\phi_p\}$ is the set of the first k KL–modes and $\{\psi_p\}$ is any other set of k orthonormal modes.

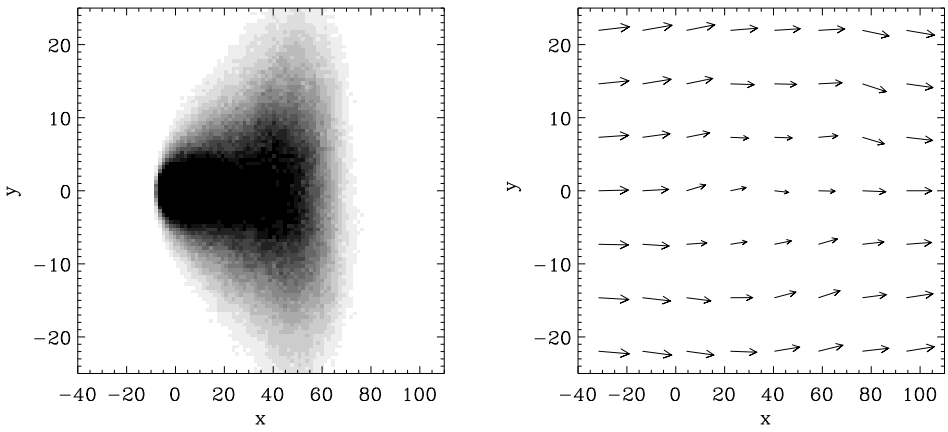

Figure 2. a) Segment density $\rho(x, y, z = 0)$ and b) time-averaged perturbed flow field $\mathbf{u}(x, y, z = 0)$ for a chain with $N = 200$ beads fixed at the origin with one end and subjected to a uniform flow in the x-direction with $v = 0.02$. Both EVI and HI are included and harmonic springs are used. The streamlines go around the region where the density of polymer segments is high.

Intuitively the KL–modes and –weights may be pictured as describing the main axes and abscissae of an ellipsoid in the data space that optimally captures the data.

Because of property 2 the KL–modes are a natural generalization of the independent eigenmodes for linear systems. Furthermore the corresponding weights may be identified with the relaxation times for nonlinear polymer models. In order to substantiate this assertion a comparison with several known results will be made in the following section.

4 Results

4.1 Partial draining effect

In this subsection we describe results obtained in simulations of a bead–spring chain which is fixed at the origin and subjected to a uniform flow in the x-direction with velocity $v = 0.02$. The chain has $N = 200$ beads connected by harmonic springs and both EV and HI are taken into account. In fig. 2a) the temporally averaged segment density is shown as a measure of the chain deformation. The full flow field $\mathbf{u}(\mathbf{r})$ including the perturbation due to the HI between the beads is shown in fig. 2b). The flow velocity assumes its smallest values near the x-axis in the interval $0 < x < 50$ where the beads are met with the largest probability. The important result from these simulations is that the flow at the average location of the polymer coil is nonvanishing. This flow penetration is a superposition of two effects: The flow penetrates the polymer coil at any moment and due to thermal fluctuations the polymer does not stay at a fixed location.

With increasing flow velocity and polymer elongation the average distance between the beads increases and therefore the hydrodynamic interaction decreases. This reduction is stronger close to the tethered end than near the free end, as long as the chain is not fully stretched. At this stage of deformation the effects of HI

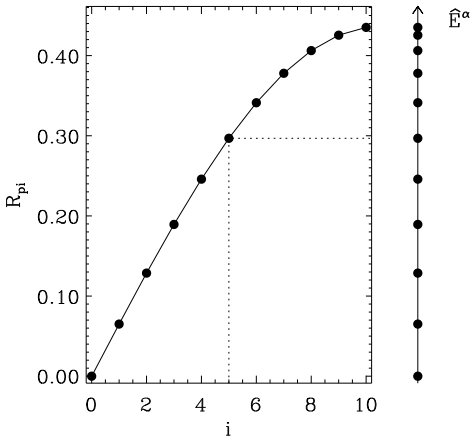

Figure 3. Illustration of the chain conformation corresponding to the first Rouse mode of a chain with $N = 10$ beads. The bead positions are on a straight line with direction $\hat{\mathbf{E}}^\alpha$ in real space as shown on the right of the plot. The diagram shows the distance of the i–th bead from the origin where the chain is fixed.

vary significantly along the polymer chain.

In recent theoretical considerations about tethered polymers the blob model with impenetrable spherical blobs has been introduced[8]. Our present simulation indicates that the assumption of complete impenetrability is too strong and has to be replaced by a partial penetration. A generalized blob model taking this and the spatially dependent HI effects into account has been suggested in Ref.[12] and elsewhere in this issue[13].

4.2 Relaxation times and modes of polymer chains

The analytical solution of the Rouse model for a chain with one end fixed and the other end free yields a relaxation spectrum[38]

$$\tau_p = \frac{\zeta}{k_H} \left(4 \sin^2 \left(\frac{2p-1}{2N+1} \frac{\pi}{2} \right) \right)^{-1} , \tag{19}$$

where $p = 1 \ldots N$ is the number of the Rouse mode. A large part of the spectrum follows a scaling law $\tau_p \propto (2p-1)^{-2}$, cf. fig. 4. Deviations from this scaling law at large mode numbers are due to the finite number of beads.

The Rouse modes $\mathbf{R}_p^\alpha$ are special chain conformations which will be described in the following. The position of the i–th bead in the mode with indices α, p may be written in the product form $\mathbf{R}_{pi}^\alpha = R_{pi} \hat{\mathbf{E}}^\alpha$. This means that all beads are on a straight line with unit direction vector $\hat{\mathbf{E}}^\alpha$ as illustrated in fig. 3. Since there are three independent directions in real space there are three possible values for α for which we may take the axes of a Cartesian coordinate system, *i.e.* $\alpha = x, y, z$. The

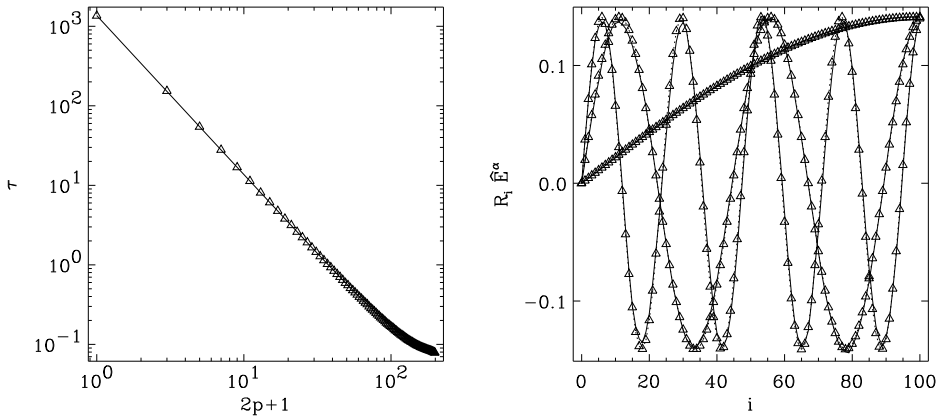

Figure 4. a) Comparison of the relaxation spectrum of the Rouse chain obtained analytically via eq. (19) (solid line) and from numerical data by means of the KL method (open triangles). On the abscissa we plot $2p+1$ instead of the mode number p alone because due to the boundary conditions with one end fixed it is only the former quantity for which a scaling law can be expected. b) Comparison of several Rouse modes ($p = 1, 5, 9$) as calculated analytically[38] (solid line) and from numerical data by means of the KL method (open triangles).

distance function

$$R_{pi} = \sqrt{\frac{2}{N}} \sin\left(i \, \frac{2p-1}{2N+1} \, \pi \right) \tag{20}$$

gives the distance of the i–th bead from the origin. There are N different patterns of bead spacings corresponding to the values $p = 1 \ldots N$.

The distance function R_{pi} is normalized according to $\sum_{i=1}^{N} R_{pi}^2 = 1$, furthermore $\sum_{i}^{N} R_{pi} R_{qi} = 0$ for $p \neq q$. Together with the orthonormality of the $\hat{\mathbf{E}}^\alpha$ in real space this expresses the orthonormality of the Rouse modes in conformation space. Since there are $3N$ modes, these form a basis for the conformation space, *i.e.* each conformation $\mathbf{R}$ may be expressed as $\mathbf{R} = \sum_{p=1}^{N} \sum_{\alpha=x,y,z} A_p^\alpha \mathbf{R}_p^\alpha$. The mode amplitude A_p^α is just a common scaling factor applied to the position vectors of all beads in the chain. The amplitudes A_p^α for the three coordinate directions in real space are often taken together as a vector amplitude $\mathbf{A}_p$.

In equilibrium none of the three directions of a Cartesian coordinate system is distinguished. Therefore the spectrum of polymer relaxation times is threefold degenerate. The modes corresponding to each triplet of relaxation times differ only in their directions $\hat{\mathbf{E}}^\alpha$ in real space while the spacing of beads along this direction is the same for all three modes in the triplet. Since no direction in space is preferred, the directions obtained by the KL method will be arbitrary.

Note that in equilibrium the average position of all beads is at the coordinate origin. In nonequilibrium the beads have in general different nonzero average positions. Since the modes serve to decompose fluctuations, $\mathbf{R}_p^\alpha$ is then to be interpreted

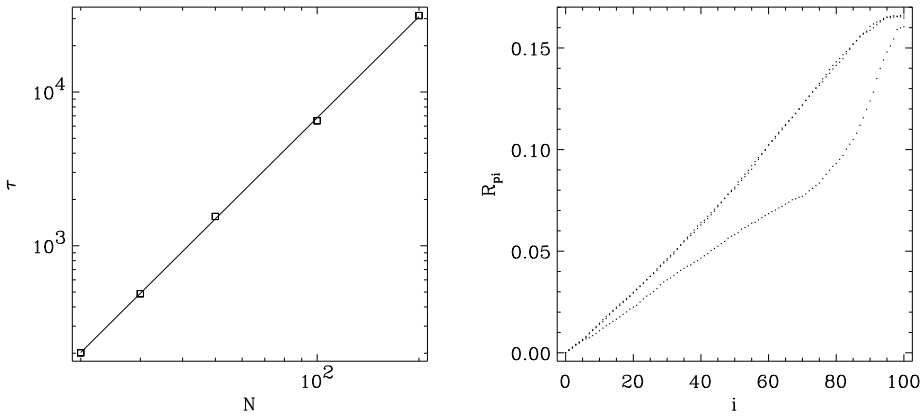

Figure 5. a) Scaling of the first (longest) relaxation time with the number of segments for a model with harmonic springs and EV. The symbols are simulation results, the solid line is a fit to a power law $\tau \propto \alpha N^{\beta}$ with the values $\alpha = -0.55108833$ and $\beta = 2.1919907$ for the fit parameters. Scaling arguments predict a value of $2\nu + 1 \approx 2.2$ for β where ν is defined in eq. (41). b) First triplet ($p = 1$) of relaxation modes as calculated by the KL–method from simulation data for a tethered FENE chain with $N = 100$ beads subjected to a uniform flow with velocity $v = 0.2$. The lower curve corresponds to the mode with direction along the flow while the two upper curves represent the two degenerate modes in perpendicular directions. Note that R_{pi} is here the deviation of the i–th bead from its mean position when the mode is excited.

as the deviation of the true bead position from its mean value.

In fig. 4 we compare the analytical results for the Rouse chain to the results of a KL–analysis as described in the previous section. The data set which was used for the analysis consisted of 10000 samples taken at time intervals of $\Delta t = 100.0$ which were generated by a simulation program using the algorithm described in section 2 and in the appendices. An initial transient of 100 samples was discarded in order to eliminate effects of the initial conformation which was $\mathbf{R}_i = i\, b\, \hat{\mathbf{E}}^x$. After this period the end–to–end distance had approached its equilibrium value of 10.0 within a statistical error of 2%. In order to obtain the above results we exploited the permutation symmetry of the coordinate axes and averaged τ_p and R_{pi} over the three coordinate directions $\hat{\mathbf{E}}^{\alpha}$. The values of the KL–weights, cf. fig. 4a), obtained for the individual coordinate directions showed deviations of less than 5% from these averages. This deviation is approximately proportional to the size of the dataset. In order to explicitly exhibit the symmetry that was averaged over before, it was necessary to increase the size of the dataset by a factor of four. If on the other hand only half of the data are used, the Rouse times of less than $\tau_p \approx 0.1$ are underestimated by the KL–method.

The KL-modes for $p = 1, 5, 9$ are shown in fig. 4b) in comparison with the analytical results for the Rouse modes. We find that approximately the first 10 % of the modes are reproduced accurately. For higher mode numbers the tips of the sine are underestimated.

A further test for the KL–approach to polymer relaxation times is furnished by the scaling law[1]

$$\tau_1 \propto N^{2\nu+1} \approx N^{2.2} \tag{21}$$

for the dependence of the longest relaxation time of a Rouse chain with EV on the number of segments. The corresponding result for the relaxation times of such a chain as calculated by the KL–method is shown in fig. 5a). The fit of a straight line to the data in the log-log plot clearly shows that the KL relaxation times do obey a power law. The exponent obtained from the fit has a value of 2.18 which is in very good agreement with the result derived from scaling arguments.

As a preliminary result for a nonequilibrium situation we show in fig. 5b) the first triplet of modes for a tethered FENE chain subjected to a uniform flow. It is obvious that the form of the modes is drasticaly changed compared to the equilibrium Rouse form. This also leads to relaxation times which depend on the flow velocity as does the precise form of the modes.

So far we only considered a tethered polymer where all degrees of freedom relax. For a freely floating polymer, however, the center–of–mass motion is diffusive. This corresponds to an infinite relaxation time which spoils the numerics. The situation is remedied easily though, by performing the KL–analysis on the bead positions *relative to the center–of–mass*. Thus the relevant case for rheological applications can also be treated with the method we suggest.

5 Conclusion

We introduced a modified Brownian dynamics scheme, cf. eq.(12), which guaratees that the equilibrium distribution is preserved during simulations, in contrast to direct discretization of eq. (5). Therefore this scheme allows the integration timestep to be chosen by a factor of 10 larger for a prescribed accuracy of the Boltzman distribution.

Simulation of the Brownian dynamics of bead–spring models for tethered polymers allows a test of the validity ranges of previous more coarse–grained model approaches as described in more detail in Ref.[10]. Furthermore a detailed study of the polymer statics and dynamics provides a starting point for the generalization and modification of these models such as the f-shell blob model for tethered polymers as introduced in Refs.[11,12,13].

Therefore this study of the behavior of tethered polymers in uniform flow is a first step in bridging the gap between the microscopic scale at which the interaction of single polymers and flow takes place and a more coares–grained description up to the macroscopic continuum dynamics of polymer solutions. Further steps leading to a thorough understanding of the non-Newtonian behavior of polymer solutions are the analysis of the nonlinear interaction of polymers with more complicated flows, *e.g.* parallel flows like shear flow and Poiseuille flow, but also extensional, curvilinear and even turbulent flow. Such an analysis may provide a basis for the formulation of the essentially nonlinear description of the macroscopic dynamics of polymer solutions. In plane Poiseuille flow, for instance, we could recently show that small deformable objects like polymers will migrate to the center where the

shear vanishes. This is another important ingredient for the theory which allows to incorporate the build-up of inhomogeneous concentration profiles of the polymer component of the solution.

Appendix

A Brownian dynamics simulation scheme

The purely dissipative equation of polymer motion eq. (5) is not appropriate for computer simulations because it does not ensure the correct Boltzmann distribution at equilibrium. However, instead of discussing the equation of motion (5) we here consider a simpler model problem, which retains only the essential difficulty of simulating overdamped stochastic equations.

As an aside we note that the noise in eq. (5) is of multiplicative nature because its strength is a function of the chain conformation via the mobility matrix $\mathbf{H}$. However, the statistical properties of the multiplicative noise are expected to depend only on the chain conformation averaged over a certain short time interval. Therefore, it is not necessary to discretize the equation of motion by treating faithfully the multiplicative nature of the thermal noise [40]. This allows us to treat the multiplicative noise as Ito type instead of treating it as Stratonovich type.

The model we use to analyse the violation of the Boltzmann distribution is

$$\Gamma(\mathbf{x})\,\dot{\mathbf{x}}(t) = -\,\frac{\partial \Phi}{\partial \mathbf{x}} + \mathbf{G}(\mathbf{x})\,\xi(t)\,, \tag{22}$$

where $\mathbf{x}$ is the N-dimensional state vector, Φ is the potential, Γ and $\mathbf{G}$ are $\mathbf{x}$-dependent square matrices and $\xi(t)$ is again the uncorrelated Gaussian white noise,

$$\left\langle \xi(t)\,\xi^T(t')\right\rangle = \delta(t-t')\,\mathbf{1}\,. \tag{23}$$

The fluctuation-dissipation relation requires that $\mathbf{G}\mathbf{G}^T = \beta^{-1}\Gamma$, where $\mathbf{G}^T$ denotes the transposed matrix of $\mathbf{G}$ and $\beta = 1/k_{\mathrm{B}}T$. In order to construct a finite difference scheme of eq. (22), we rewrite it as

$$\dot{\mathbf{x}}(t) = -\,\Gamma^{-1}(\mathbf{x})\,\frac{\partial \Phi}{\partial \mathbf{x}} + \tilde{\mathbf{G}}(\mathbf{x})\,\xi(t). \tag{24}$$

where $\tilde{\mathbf{G}} \equiv \Gamma^{-1}\mathbf{G}$. As mentioned above, we regard the multiplicative nature of the noise only in a time-averaged sense, which allows us to construct a finite difference scheme of eq. (24) that is correct up to $O(h)$ as[41,40]

$$\mathbf{x}(t_n+h) - \mathbf{x}(t_n) = -\,\Gamma^{-1}(\mathbf{x}(t_n))\,\frac{\partial \Phi}{\partial \mathbf{x}(t_n)}\,h + \tilde{\mathbf{G}}(\mathbf{x}(t_n))\,\Xi(t_n)\,\sqrt{h} + O(h^{3/2})\,, \tag{25}$$

where h is the time step of the integration and $t_n \equiv nh$ is the time at the beginning of the n-th time step. The discretized white noise Ξ is again an N-vector of independent Gaussian random numbers with zero mean and unit variance, *i.e.*

$$\left\langle \Xi(t_n)\;\Xi^T(t_{n'})\right\rangle = \delta_{nn'}\,\mathbf{1}\,. \tag{26}$$

In thermal equilibrium, the probability distribution for the variable $\mathbf{x}$ is given by the canonical distribution $\exp(-\beta\Phi(\mathbf{x}))$ which remains unchanged by the time evolution

of the system according to the equation of motion (22). In order not to violate a fundamental physical principle, the finite difference scheme eq. (25) should also preserve the canonical distribution up to $O(h)$, which is checked in the following. Using eqs. (25) and (26), we can calculate the probability distribution of finding $\mathbf{y} = \mathbf{x}(t_n + h)$ under the condition that we had $\mathbf{z} = \mathbf{x}(t_n)$ as

$$\begin{aligned} \langle \mathbf{y} \rangle &= \mathbf{z} - \Gamma^{-1}(\mathbf{z}) \, \frac{\partial \Phi}{\partial \mathbf{z}} \, h + O(h^{3/2}) \\ \left\langle \left(\mathbf{y} - \langle \mathbf{y} \rangle \right) \left(\mathbf{y} - \langle \mathbf{y} \rangle \right)^T \right\rangle &= \beta^{-1} \, \Gamma(\mathbf{z}) \, h + O(h^{3/2}) \, . \end{aligned} \tag{27}$$

Due to the linearity of eq. (25) and the Gaussian nature of the random vector $\Xi(t_n)$, the probability distribution of $\mathbf{x}(t_n+h)$ becomes a Gaussian distribution, too. Using eq. (27), the probability distribution of $\mathbf{y} = \mathbf{x}(t_n + h)$ under the condition of $\mathbf{z}$ is given by

$$\mathcal{P}\left(\mathbf{y}|\mathbf{z}\right) = \left(\left(\frac{2\pi h}{\beta} \right)^N \det\!\left(\Gamma^{-1}(\mathbf{z})\right) \right)^{-\frac{1}{2}} \exp\!\left(-\frac{\beta}{2h} \, \left(\mathbf{y} - \bar{\mathbf{y}} \right)^T \Gamma(\mathbf{z}) \, \left(\mathbf{y} - \bar{\mathbf{y}} \right) \right) \tag{28}$$

with

$$\bar{\mathbf{y}} = \mathbf{z} - \Gamma^{-1}(\mathbf{z}) \, \frac{\partial \Phi}{\partial \mathbf{z}} \, h \, . \tag{29}$$

Then the time–invariance of the canonical distribution is expressed as

$$\exp\!\left(-\beta \, \Phi(\mathbf{y}) \right) = \int d\mathbf{z} \, \exp\!\left(-\beta \, \Phi(\mathbf{z}) \right) \mathcal{P}(\mathbf{y}|\mathbf{z}) \, . \tag{30}$$

If the condition eq. (30) is violated, the canonical distribution is no longer accurately fulfilled and the scheme eq. (25) cannot guarantee the existence of the correct equilibrium state. Expanding eq. (30) in a power series in the time step h, one easily confirms that the leading order of the numerical error in the condition eq. (30) associated with the time discretization is linear in h. As this error is larger than the truncation error in the numerical scheme eq.(25), the equilibrium condition is not accurate up to leading orders.

One way to eliminate the difficulty of the violation of the stable equilibrium state is to extend the equation of motion eq. (22) to a second order differential equation by including an artificial inertial term. Then the equation of motion reads

$$m \ddot{\mathbf{x}}(t) + \Gamma(\mathbf{x}) \, \dot{\mathbf{x}}(t) = - \frac{\partial \Phi}{\partial \mathbf{x}} + \mathbf{G}(\mathbf{x}) \, \xi(t) \, , \tag{31}$$

where the artificial mass m is taken identical for all the components of $\mathbf{x}$ for simplicity. In this case, the finite difference time integration scheme that is correct up to $O(h)$, is given by

$$\begin{aligned} \mathbf{y} &= \mathbf{z} + \mathbf{v}(t_n) \, h + O(h^{3/2}) \\ m\mathbf{v}(t_n + h) &= m\mathbf{v}(t_n) + \mathbf{G}\left(\mathbf{z}\right) \Xi(t_n) \, \sqrt{h} - \left(\frac{\partial \Phi}{\partial \mathbf{z}} + \Gamma(\mathbf{z}) \, \mathbf{v}(t_n) \right) h + O(h^{3/2}) \end{aligned} \tag{32}$$

where $\mathbf{v} \equiv \dot{\mathbf{x}}$ is the velocity and $\mathbf{z} = \mathbf{x}(t_n)$. Introducing $\mathbf{y} = \mathbf{x}(t_n + h)$, $\mathbf{u} = \mathbf{v}(t_n + h)$ and $\mathbf{w} = \mathbf{v}(t_n)$, and using eq. (26), we find

$$\begin{aligned}
\langle \mathbf{y} \rangle &= \mathbf{z} + \mathbf{w}\, h + O(h^{3/2}) \equiv \bar{\mathbf{y}} + O(h^{3/2}) \\
m\langle \mathbf{u} \rangle &= m\mathbf{w} - \left(\frac{\partial \Phi}{\partial \mathbf{z}} + \Gamma(\mathbf{z})\, \mathbf{w} \right) h + O(h^{3/2}) \\
&\equiv m\bar{\mathbf{u}} + O(h^{3/2}) \\
\left\langle \left(\mathbf{y} - \langle \mathbf{y} \rangle\right) \left(\mathbf{y} - \langle \mathbf{y} \rangle\right)^T \right\rangle &= O(h^{3/2}) \\
\left\langle \left(\mathbf{u} - \langle \mathbf{u} \rangle\right) \left(\mathbf{u} - \langle \mathbf{u} \rangle\right)^T \right\rangle &= \beta^{-1}\Gamma(\mathbf{z})\, h + O(h^{3/2}) \\
\left\langle \left(\mathbf{y} - \langle \mathbf{y} \rangle\right) \left(\mathbf{u} - \langle \mathbf{u} \rangle\right)^T \right\rangle &= O(h^{3/2})
\end{aligned} \tag{33}$$

Then, the probability distribution of finding $(\mathbf{y}, \mathbf{u})$ under the condition $(\mathbf{z}, \mathbf{w})$ is given by

$$\mathcal{P}\left(\mathbf{y}, \mathbf{u} | \mathbf{z}, \mathbf{w}\right) = \left(\left(\frac{2\pi h}{\beta} \right)^N \det\left(\Gamma^{-1}(\mathbf{z})\right) \right)^{-\frac{1}{2}} \exp\left(-\frac{\beta}{2h} \left(\mathbf{u} - \bar{\mathbf{u}}\right)^T \Gamma(\mathbf{z}) \left(\mathbf{u} - \bar{\mathbf{u}}\right) \right) \delta\left(\mathbf{y} - \bar{\mathbf{y}}\right) \tag{34}$$

where $\bar{\mathbf{y}}$ and $\bar{\mathbf{u}}$ are defined in eq. (33). With this equation one can construct a balance equation for the equilibrium canonical distribution that is similar to eq. (30),

$$\exp\left(-\beta \left(\Phi(\mathbf{y}) + \frac{1}{2} m \left|\mathbf{u}\right|^2 \right) \right) = \int d\mathbf{z}\, d\mathbf{w}\, \exp\left(-\beta \left(\Phi(\mathbf{z}) + \frac{1}{2} m \left|\mathbf{w}\right|^2 \right) \right) \mathcal{P}\left(\mathbf{y}, \mathbf{u} | \mathbf{z}, \mathbf{w}\right) . \tag{35}$$

Expanding eq. (35) with respect of h, one can confirm that the discretization error in the balance condition is of the order as $O(h^2)$, which is smaller than the truncation error in the difference scheme eq. (32).

B Efficient Evaluation of Stochastic Forces in the Presence of HI

A key issue for the present study with emphasis on HI is the calculation of the matrix $\sqrt{\mathbf{H}}$ in eq. (5) and eq. (12). In order to make the whole algorithm practical, an efficient way to evaluate the square root of the mobility matrix $\mathbf{H}$ must be developed. The straight forward calculation of such an expression[42] involves a diagonalization of $\mathbf{H}$ which numerically requires an effort of $\mathcal{O}(N^3)$ machine instructions. A second standard method for the calculation of matrix functions is via series expansion of the desired function[42]. A Taylor series will contain only powers of the matrix argument which are easily evaluated numerically. However, matrix multiplication also requires $\mathcal{O}(N^3)$ operations. A third method which again needs $\mathcal{O}(N^3)$ operations but which offers the most favorable prefactor becomes possible by noting that the square root is not precisely what is needed. Instead one can also use the Cholesky decomposition of $\mathbf{H}$. This idea was exploited in the classic work by Ermak & McCammon[43]. In all cases the numerical effort of $\mathcal{O}(N^3)$ makes the computation prohibitive for long chains. Therefore to our knowledge all previous

BD studies of polymer dynamics which took HI into account were limited to chains with $N \leq 20$ beads with one exception, the work of Fixman[44], where a few results for a chain of 56 beads are given.

An approximate method which requires only $\sim \mathcal{O}(N^{2.25})$ operations was proposed by Fixman[45]. The starting point for this method is an expression of the square root in terms of a complete set of polynomials as in method two above, *i.e.*

$$\sqrt{\mathbf{H}} = \sum_{\mu=1}^{M} \mathcal{P}^{\mu}(\mathbf{H})\,. \tag{36}$$

A reduction of the computational effort becomes possible by noting that the knowledge of the matrix $\sqrt{\mathbf{H}}$ is actually much more than what is really needed since once it is known it could be applied to many different random vectors ξ. For the simulation however it needs to be applied to *one single* realization only. A scheme which takes advantage of this is obtained by multiplying both sides of eq. (36) with ξ. Taking ξ into the sum on the *rhs* one obtains a series expression for $\sqrt{\mathbf{H}}\,\xi$

$$\sqrt{\mathbf{H}}\,\xi = \sum_{\mu=1}^{M} \mathcal{P}^{\mu}(\mathbf{H})\,\xi\,. \tag{37}$$

This expression contains only matrix–vector products and thus its evaluation requires an effort of $\mathcal{O}(N^2)$ only. Furthermore the individual terms in the sum may be calculated recursively keeping the number of these operations low, too.

The polynomials $\mathcal{P}^{\mu}(x)$ may be taken from *any* complete set in function space. The most economic choice are not simple powers $\mathcal{P}^{\mu}(x) = x^{\mu}$ but Chebychev polynomials $C^{\mu}(x)$[46,47]. These can be evaluated by means of the recursion relation

$$C^{\mu+1}(x) = 2\,x\,C^{\mu}(x) - C^{\mu-1}(x)\,, \tag{38}$$

$$\text{with} \qquad C^{1}(x) = x\,,$$

$$\text{and} \qquad C^{0}(x) = 1\,. \tag{39}$$

Since the Chebychev polynomials are defined on the interval $[-1,1]$, which is not suitable in the present context, one applies a transformation of the independent variable

$$x = \frac{2y}{b-a} - \frac{b+a}{b-a}\,, \tag{40}$$

which maps the domain of the problem $y \in [a,b]$ to the domain $x \in [-1,1]$ of the Chebychev polynomials. The $C^{\mu}(y)$ appear frequently in numerical analysis and are referred to as shifted Chebychev polynomials[46,47].

If, as in the problem under consideration, the argument x is a matrix, not a simple scalar, then $[a,b]$ is the range of eigenvalues of x. An estimate of the range of the eigenvalues of $\mathbf{H}$ is furnished by a simple physical argument: If two nearby beads experience a force in the same direction, the induced perturbations of the velocity field will have a large degree of coherence and thus add up to a larger perturbation while if the forces are in opposite directions, the induced perturbations will cancel out to a large extent. Since beads which are neighbors along the chain are likely to be also close in space, an estimate for the largest eigenvalue is

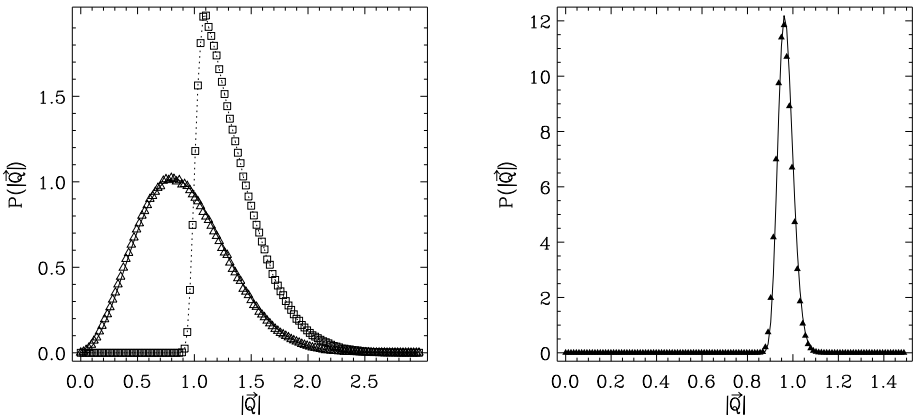

Figure 6. Probability distribution for the bond length $|\mathbf{Q}| = |\mathbf{R}_{j+1} - \mathbf{R}_j|$ at thermal equilibrium for models with a) harmonic springs, both with (triangles) and without (squares) EV, and b)FENE springs. In the latter case the addition of EV has no effect on the bond length distribution since nearest–neighbor repulsion is included in the spring potential anyways. The solid lines are obtained by evaluating the Boltzmann factor $\exp(-\Phi/k_{\rm B}T)$ with the potentials given by eq. (6) for the Rouse model (left) and eq. (7) for the FENE model (right). In the latter case there is no difference between the case with and without EV as far as the bond lengths are concerned. The symbols give the results of the corresponding simulations for a chain with $N = 100$ beads. From the distribution data the mean bond length is calculated as $b = 1.33$ for the Rouse model with EV and as $b = 0.965$ for the FENE model.

obtained by using a force vector with equal forces for all beads as a testvector $\mathbf{F}$ to form the Rayleigh quotient[42] $\mathbf{F}^T\,\mathbf{H}\,\mathbf{F}/\mathbf{F}^T\,\mathbf{F}$. Similarly an estimate for the smallest eigenvalue is obtained by using a force vector with alternating forces for all beads as a testvector. In order to compensate for deviations of these estimates from the true values of largest and smallest eigenvalue of $\mathbf{H}$ one takes a somewhat larger interval for the shifted Chebychev polynomials.

The order of truncation of the series, M, has to be determined empirically and increases somewhat with N whence the final effort goes with a somewhat higher power than 2. In order to monitor the accuracy of the approximation we compute the exact square root of $\mathbf{H}$ via the spectral theorem using a QR algorithm[42] for the diagonalization whenever the conformation is saved. This happens only every 100 - 10000 timesteps of the integration and is thus acceptable in terms of computer time.

C Program tests

At thermal equilibrium the simulations can be compared with several well-known analytical results. The equilibrium distribution of the bond lengths can be calculated via the Boltzmann factor $\exp(-\Phi/k_BT)$ using the spring potentials given in sec. 2. These analytically calculated distributions are compared in fig. 6 with the

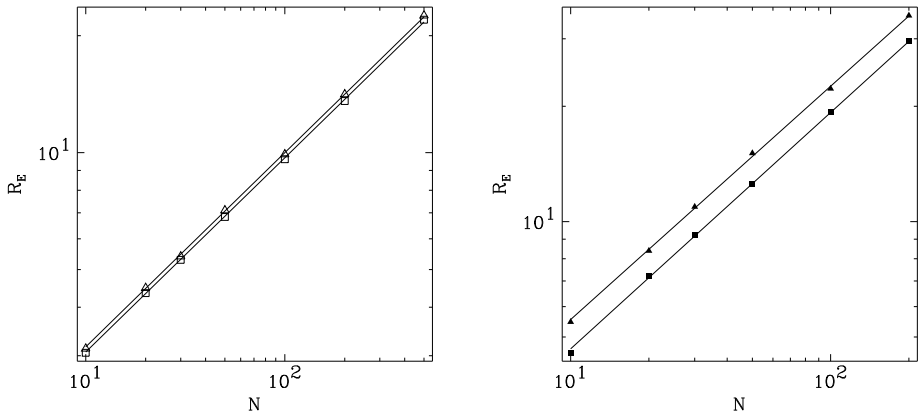

Figure 7. a) Equilibrium scaling of the end–to–end distance R_E with the number of segments N for the Rouse (open triangles) and FENE models (open squares). The solid lines are due to the scaling relation $R_E = b\sqrt{N}$, with the mean bond length $b = 1.0$ for the Rouse chain and $b = 0.961$ for the FENE chain. b) Equilibrium scaling of the end–to–end distance with the number of segments for the Rouse (solid triangles) and FENE models (solid squares) including the excluded volume effect. The solid lines are fits with a power law $R_E = bN^{\nu}$. The fit parameters are $\nu = 0.602$, $b = 1.37$ for the Rouse model and $\nu = 0.617$, $b = 1.13$ for the FENE model.

distributions obtained from simulations using these potentials for the springs.

For the Rouse model the bond length distribution is of course a Maxwellian. For the FENE model the distribution is sharply peaked around its maximum value so that it can be regarded as a good approximation to a freely jointed chain model. The bond length distribution for the Rouse model with excluded volume interactions reveals that the repulsive potential acts as a rather hard wall. Hence the distribution is deformed and its mean value is shifted to larger values. The addition of the excluded volume interactions to the FENE model of course leaves the bond length distribution unchanged because nearest neighbor repulsion is included anyways as described in section 2. As the analysis of the scaling of the end–to–end distance with the number of segments shows (see below), the effective bond length is rather close to the distance $b = 0.961$ where the bond length distribution has its maximum.

A second more global test is the comparison of the numerically obtained end-to-end distance R_E as a function of the number of segments N with the scaling result due to Flory[48]

$$R_E = bN^{\nu} \,. \tag{41}$$

Here ν is the scaling exponent while b may be interpreted as an effective bond length. For any model with purely local interactions between the beads it is well known that the exponent is $\nu = 1/2$[3]. In fig. 7a) we verify this behavior for the pure Rouse and FENE models. In these cases of course also the bond lengths are known so that we can contrast the numerical values with an analytical result without any adjustable parameters. The small difference between both models comes from the

fact that the bond lengths for the Rouse ($b = 1.0$) and FENE model ($b = 0.961$) are slightly different. For both models there is a very good agreement with the numerical data even for rather short chains.

The excluded volume interactions change the scaling exponent for R_{E} from $\nu = 1/2$ to $\nu = 3/5$ neglecting a small correction to mean field theory[48]. In fig. 7b) we verify this behavior for the Rouse and FENE models with EV. Since the prefactor is not known we fit a power law of the form of eq. (41) to the numerical data. The values of the exponents are $\nu \sim 0.6$ for the models with either harmonic or FENE springs, which is in quite good agreement with the theoretical values. For the model with harmonic springs, the repulsive potential due to the excluded volume interaction leads to a considerable shift of the mean bond length to $b = 1.366$.

For the models with hydrodynamic interactions, a test is possible since all static properties at equilibrium are determined solely by the potential Φ whereas the hydrodynamic interactions affect only the mobility. So one can simply compare the numerical values of the above quantities for the models with and without the hydrodynamic effects. We find agreement within the statistical errors.

References

1. P.-G. d. Gennes, *Scaling Concepts in Polymer Physics* (Cornell University Press, Ithaca, 1981).
2. R. B. Bird, R. C. Armstrong, and O. Hassager, *Dynamics of Polymeric Liquids, Vols.* I, II, 2nd ed. (John Wiley & Sons, New York, 1987), .
3. M. Doi and S. F. Edwards, *The Theory of Polymer Dynamics* (Clarendon Press, Oxford, 1986), .
4. T. T. Perkins, S. R. Quake, D. E. Smith, and S. Chu, Science **264**, 822 (1994).
5. T. T. Perkins, D. E. Smith, R. G. Larson, and S. Chu, Science **268**, 83 (1995).
6. S. Manneville *et al.*, Europhys. Lett. **36**, 413 (1996).
7. T. T. Perkins, D. E. Smith, and S. Chu, Science **276**, 2016 (1997).
8. F. Brochard-Wyart, Europhys. Lett. **23**, 105 (1993).
9. F. Brochard-Wyart, Europhys. Lett. **30**, 387 (1995).
10. R. Rzehak, W. Kromen, T. Kawakatsu, and W. Zimmermann, Deformations of a Tethered Polymer in Uniform Flow, 1999, in preparation.
11. R. Rzehak, T. Kawakatsu, D. Kienle, and W. Zimmermann, Partial Draining for a Tethered Polymer in Flow, 1999, submitted to Europhys. Lett.
12. D. Kienle and W. Zimmermann, F-shell Blob Model for a Tethered Polymer in Strong Flows, 1999, in preparation.
13. D. Kienle, R. Rzehak, and W. Zimmermann, F-shell Blob Model Inspired by Simulations of Tethered Polymers, 1999, this issue.
14. H. C. Öttinger, J. Chem. Phys. **86**, 3731 (1987).
15. J. J. Magda, R. G. Larson, and M. E. Mackay, J. Chem. Phys. **89**, 2504 (1988).
16. R. G. Larson, T. T. Perkins, D. E. Smith, and S. Chu, Phys. Rev. E **55**, 1794 (1997).
17. J. D. Ferry, *Viscoelastic Properties of Polymers*, 3rd ed. (John Wiley & Sons, New York, 1964).

18. P. E. Rouse, jr, J. Chem. Phys. **21**, 1272 (1953).
19. B. H. Zimm, J. Chem. Phys. **24**, 269 (1956).
20. B. H. Zimm, G. M. Roe, and L. F. Epstein, J. Chem. Phys. **24**, 279 (1965).
21. H. C. Öttinger and W. Zylka, J. Rheol. **36**, 885 (1992).
22. H. C. Öttinger, *Stochastic Processes in Polymeric Fluids* (Springer, Heidelberg, 1996).
23. S. W. Provencher, Comp. Phys. Commun. **27**, 213 (1982).
24. C. Elster and J. Honerkamp, J. Rheol. **36**, 911 (1992).
25. M. Loève, *Probability Theory* (van Nostrand, Princeton, 1955).
26. R. B. Bird and H. C. Öttinger, Annu. Rev. Phys. Chem. **43**, 371 (1992).
27. H. Yamakawa, *Modern Theory of Polymer Solutions* (Harper & Row, New York, 1971), .
28. J. D. Schieber and H. C. Öttinger, J. Chem. Phys. **89**, 6972 (1988).
29. H. R. Warner, jr, Ind. Eng. Chem. Fundam. **11**, 379 (1972).
30. K. Kremer and G. S. Grest, J. Chem. Phys. **92**, 5057 (1990).
31. R. Zwanzig, Adv. Chem. Phys. **15**, 325 (1969).
32. W. Zylka and H. C. Öttinger, J. Chem. Phys. **90**, 474 (1989).
33. H. C. Öttinger and Y. Rabin, J. Rheol. **33**, 725 (1989).
34. T. Schneider and E. Stoll, Phys. Rev. B **17**, 1302 (1978).
35. R. W. Preisendorfer and C. D. Mobley, *Principal Component Analysis in Meteorology and Oceanography* (Elsevier, Amsterdam, 1988).
36. L. Sirovich and R. Everson, International Journal of Supercomputer Applications **6**, 50 (1992).
37. J. L. Lumley, *Stochastic Tools in Turbulence* (Academic Press, New York, 1970).
38. R. Rzehak and W. Zimmermann, Relaxation Modes and –Times for Nonlinear Polymer Models and the Karhunen–Loève Method, 1999, in preparation.
39. G. Berkooz, in *Studies in Turbulence*, edited by T. B. Gatski, S. Sarkar, and C. Speziale (Springer, Heidelberg, 1992).
40. J. M. Sancho, M. S. Miguel, S. L. Katz, and J. D. Gunton, Phys. Rev. A **26**, 1589 (1982).
41. M. P. Allen and D. J. Tildesley, *Computer Simulation of Liquids* (Clarendon Press, Oxford, 1987), .
42. G. H. Golub and C. F. v. Loan, *Matrix Computations*, 2nd ed. (John Hopkins University Press, Baltimore MD, 1989).
43. D. L. Ermak and J. A. McCammon, J. Chem. Phys. **69**, 1352 (1978).
44. M. Fixman, Macromolecules **19**, 1195 (1986).
45. M. Fixman, Macromolecules **19**, 1204 (1986).
46. A. Björck and G. Dahlquist, *Numerische Methoden*, 2nd ed. (R. Oldenbourg, München, 1979).
47. W. H. Press *et al.*, *Numerical recipes in C*, 3rd ed. (Cambridge University Press, Cambridge, UK, 1990).
48. P. J. Flory, *Statistical Mechanics of Chain Molecules* (Interscience Publishers, New York, 1969).